



HAL
open science

Combination of electrospray ionization, atmospheric pressure photoionization and laser desorption ionization Fourier transform ion cyclotronic resonance mass spectrometry for the investigation of complex mixtures – Application to the petroleomic analysis of bio-oils

Jasmine Hertzog, Vincent Carré, Yann Le Brech, Colin Logan Mackay,
Anthony Dufour, Ondřej Mašek, Frederic Aubriet

► **To cite this version:**

Jasmine Hertzog, Vincent Carré, Yann Le Brech, Colin Logan Mackay, Anthony Dufour, et al.. Combination of electrospray ionization, atmospheric pressure photoionization and laser desorption ionization Fourier transform ion cyclotronic resonance mass spectrometry for the investigation of complex mixtures – Application to the petroleomic analysis of bio-oils. *Analytica Chimica Acta*, 2017, 969, pp.26-34. 10.1016/j.aca.2017.03.022 . hal-01930182

HAL Id: hal-01930182

<https://hal.univ-lorraine.fr/hal-01930182>

Submitted on 5 Mar 2024

HAL is a multi-disciplinary open access archive for the deposit and dissemination of scientific research documents, whether they are published or not. The documents may come from teaching and research institutions in France or abroad, or from public or private research centers.

L'archive ouverte pluridisciplinaire **HAL**, est destinée au dépôt et à la diffusion de documents scientifiques de niveau recherche, publiés ou non, émanant des établissements d'enseignement et de recherche français ou étrangers, des laboratoires publics ou privés.



Distributed under a Creative Commons Attribution - NonCommercial - NoDerivatives 4.0 International License



THE UNIVERSITY *of* EDINBURGH

Edinburgh Research Explorer

Combination of electrospray ionization, atmospheric pressure photoionization and laser desorption ionization Fourier transform ion cyclotronic resonance mass spectrometry for the investigation of complex mixtures - Application to the petroleomic analysis of bio-oils

Citation for published version:

Hertzog, J, Carre, V, Le Brech, Y, Mackay, CL, Dufour, A, Masek, O & Aubriet, F 2017, 'Combination of electrospray ionization, atmospheric pressure photoionization and laser desorption ionization Fourier transform ion cyclotronic resonance mass spectrometry for the investigation of complex mixtures - Application to the petroleomic analysis of bio-oils', *Analytica Chimica Acta*.
<https://doi.org/10.1016/j.aca.2017.03.022>

Digital Object Identifier (DOI):

[10.1016/j.aca.2017.03.022](https://doi.org/10.1016/j.aca.2017.03.022)

Link:

[Link to publication record in Edinburgh Research Explorer](#)

Document Version:

Peer reviewed version

Published In:

Analytica Chimica Acta

General rights

Copyright for the publications made accessible via the Edinburgh Research Explorer is retained by the author(s) and / or other copyright owners and it is a condition of accessing these publications that users recognise and abide by the legal requirements associated with these rights.

Take down policy

The University of Edinburgh has made every reasonable effort to ensure that Edinburgh Research Explorer content complies with UK legislation. If you believe that the public display of this file breaches copyright please contact openaccess@ed.ac.uk providing details, and we will remove access to the work immediately and investigate your claim.



1 **Combination of electrospray ionization, atmospheric pressure**
2 **photoionization and laser desorption ionization Fourier transform ion**
3 **cyclotronic resonance mass spectrometry for the investigation of complex**
4 **mixtures – Application to the petroleomic analysis of bio-oils**

5
6
7 Jasmine Hertzog ¹, Vincent Carré¹, Yann Le Brech², Colin Logan Mackay³, Anthony Dufour², Ondřej
8 Mašek⁴, Frédéric Aubriet¹

- 9
10 1 LCP-A2MC, FR 2843 Institut Jean Barriol de Chimie et Physique Moléculaires et Biomoléculaires,
11 FR 3624 Réseau National de Spectrométrie de Masse FT-ICR à très haut champ, Université de
12 Lorraine, ICPM, 1 boulevard Arago, 57078 Metz Cedex 03, France
13 2 LRGP, CNRS, Université de Lorraine, ENSIC, 1, Rue Grandville, 54000 Nancy, France
14 3 SIRCAMS, School of Chemistry, University of Edinburgh, Edinburgh, EH9 3FJ, Scotland, United
15 Kingdom
16 4 UK Biochar Research Center, School of Geosciences, University of Edinburgh, Kings Buildings,
17 Edinburgh, EH9 3JN, UK
18

19
20 **Corresponding authors**

21
22 **Frédéric Aubriet**

23 frederic.aubriet@univ-lorraine.fr

24 phone (33) 3 72 74 9 34

25 LCP–A2MC

26 ICPM,

27 1 boulevard Arago,

28 57078 Metz Cedex 03, France

29
30 **Vincent Carré**

31 vincent.carre@univ-lorraine.fr

32 phone (33) 3 72 74 9 33

33 LCP–A2MC

34 ICPM,

35 1 boulevard Arago,

36 57078 Metz Cedex 03, France

37

1 **ABSTRACT**

2 The comprehensive description of complex mixtures such as bio-oils is required to
3 understand and improve the different processes involved during biological, environmental or
4 industrial operation. In this context, we have to consider how different ionization sources can
5 improve a non-targeted approach. Thus, the Fourier transform ion cyclotron resonance mass
6 spectrometry (FT-ICR MS) has been coupled to electrospray ionization (ESI), laser desorption
7 ionization (LDI) and atmospheric pressure photoionization (APPI) to characterize an oak pyrolysis bio-
8 oil. Close to 90% of the all 4500 compound formulae has been attributed to $C_xH_yO_z$ with similar
9 oxygen class compound distribution. Nevertheless, their relative abundance in respect with their
10 double bond equivalent (DBE) value has evidenced significant differences depending on the ion
11 source used. ESI has allowed compounds with low DBE but more oxygen atoms to be ionized. APPI
12 has demonstrated the efficient ionization of less polar compounds (high DBE values and less oxygen
13 atoms). The LDI behavior of bio-oils has been considered intermediate in terms of DBE and oxygen
14 amounts but it has also been demonstrated that a significant part of the features are specifically
15 detected by this ionization method. Thus, the complementarity of three different ionization sources
16 has been successfully demonstrated for the exhaustive characterization by petroleomic approach of
17 a complex mixture.

18

19 **KEYWORDS**

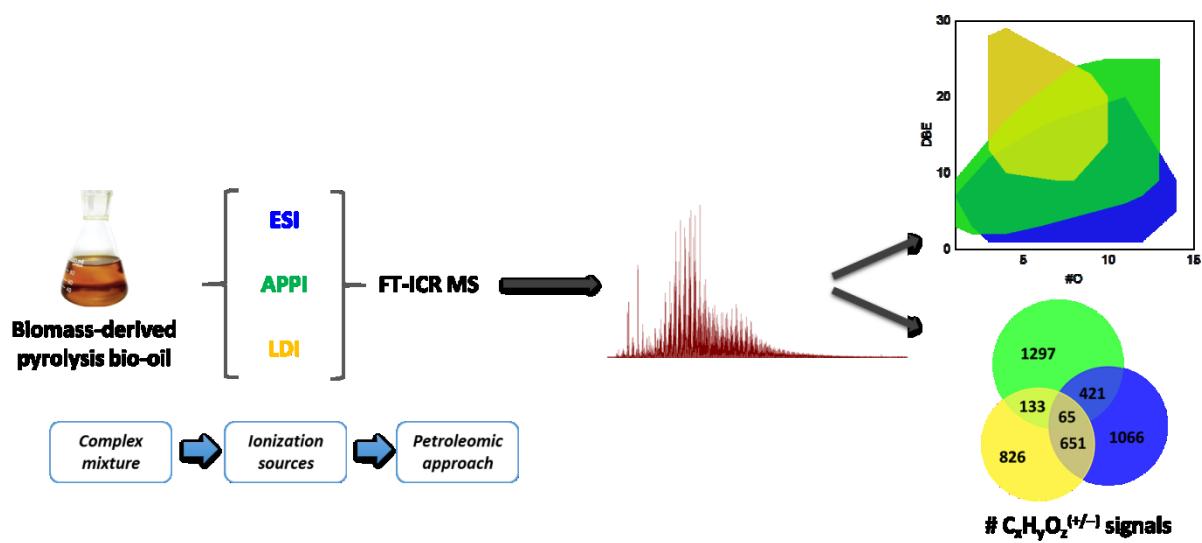
20 Non-targeted analysis, bio-oils, petroleomic approach, Ultra-high resolution mass
21 spectrometry.

22

23 **HIGHLIGHTS**

- 24 • Non-targeted mass spectrometry approach by combining electrospray ionization,
25 atmospheric pressure photoionization and laser/desorption ionization.
26 • Exhaustive description of pyrolytic bio-oil components.
27 • Distinction of sugarc derivatives, lignin derivatives and lipids contained in a woody-based
28 pyrolytic bio-oil.

1 GRAPHICAL ABSTRACT



2

3

Color for online only

1 1. INTRODUCTION

2 The analysis of complex mixtures by mass spectrometry is currently still a challenge. Different
3 methodologies may be used. The first category involves a targeted analysis using the combination of
4 mass spectrometry with liquid or gas chromatography, which is limited to known class of compounds
5 [1–4]. The second category, capable of a broader description of a complex mixture, includes non-
6 targeted analysis methods, such as petroleomic or metabolomic approaches. Some works use gas or
7 liquid chromatography [5,6], but the main part of non-targeted analyses in the field of petroleomic is
8 performed without separation prior the acquisition of the mass spectrum. Therefore, it requires the
9 use of ultra-high mass resolution and accurate mass measurement analysis due to the absence of
10 separation prior the acquisition of the mass spectrum. Fourier transform ion cyclotron resonance
11 mass spectrometry (FT-ICR MS) [7–11] and in a lesser extent the Fourier transform Orbitrap mass
12 spectrometry (FT-Orbitrap MS) [12–14] represent techniques from the second category. These
13 techniques offer numerous advantages as an exhaustive description of complex mixtures and the
14 reduced time of data acquisition, but also suffer from several drawbacks. The key obstacle in non-
15 target analysis is the ionization competition effect, which ensures the detection of easy ionized
16 species (not always the most abundant) at the expense of other mixture components. The
17 combination of different ionization techniques such as electrospray (ESI), laser desorption (LDI) and
18 atmospheric pressure photoionization (APPI) as well as the analysis of positive and negative ions may
19 overcome this problem [15–17].

20 Pyrolysis bio-oil is a good example of a highly complex mixture made up of thousands of
21 compounds with differing properties [18]. Furthermore, their composition changes depending on the
22 raw feedstocks and the conditions employed for their production and/or the catalytic treatment
23 carried out prior to their use as bio-fuel [19,20]. Indeed, pyrolysis bio-oil components are too
24 oxygenated to allow their direct use as a fuel and require catalytic treatment to remove the main
25 part of the oxygen atoms. Exhaustive and accurate characterization is required to improve, the
26 pyrolysis process itself and the catalytic treatment efficiency [21–24]. This can be achieved through
27 application of the petroleomic non-targeted approach with FT-ICR MS [25–27] or FT-Orbitrap MS
28 [28,29], whereby a part of the total composition of bio-oil can be elucidated.

29 The majority of published studies dealing with the characterization of pyrolysis bio-oils by FT-
30 ICR MS were conducted using ESI typically in negative ion mode. Different sample preparations (with
31 or without fractionation of the sample) or the addition of dopant to increase the ionization yield have
32 been reported. Miettinen *et al.* [30] and Jarvis *et al.* [31] have analyzed the aqueous and oily phases
33 of different pyrolysis bio-oil after fractionation. In both studies, the heteroatom class distributions
34 showed larger amounts of highly oxygenated compounds in the aqueous fraction than in the oily

1 phase. The authors concluded that the aqueous phase is mainly composed of “sugarc species”;
2 whereas the oily phase is composed of lipids and pyrolytic lignin derivatives. A more exhaustive
3 fractionation method was used by Liu *et al.* [32] to fully characterize by (–) ESI FT-ICR MS the
4 pyrolytic bio-oil of red pine. The least polar fractions of bio-oil were not ionized when the raw bio-oil
5 was infused in the ESI source due to ionization extinction effect. We recently proposed the use of
6 different dopants to improve ionization efficiency in (+/–) ESI FT-ICR MS [33]. In that case, it was
7 possible to detect on the same mass spectrum, without fractionation, the bio-oil components of the
8 aqueous and oily phases. The effect of alternative dopants in (–) ESI FT-ICR MS has been
9 demonstrated to improve deprotonation (addition of NH₄OH [15,25,26] or NaOH [15]) or to favor the
10 formation of [M+Cl][–] adduct ion (NH₄Cl dopant) [15]. In (+) ESI FT-ICR MS, formic acid and NH₄Cl
11 (formation of [M+H]⁺) or NaCl (generation of [M+Na]⁺ sodiated ion) ions have been used [15].
12 Regardless of these advances, ESI exhibits poor ionization of non-polar compounds. The use of LDI or
13 APPI has been previously proposed to detect these non- or poorly-ionized bio-oil components.

14 Cole *et al.* [28] investigated nitrogen species from raw switch grass pyrolysis bio-oils using ESI
15 and APPI FT-Orbitrap MS and have shown that N₁ and N₂ compounds are the dominant species
16 observed with (+) ESI FT-Orbitrap MS whereas with (+) APPI FT-Orbitrap MS the majority were
17 oxygen-containing species. They also characterized the less complex toluene extracts from biochar by
18 FT-Orbitrap MS with ESI, APPI and LDI sources [17]. Leonadis *et al.* [34] investigated the less polar
19 bio-oil components (aromatic and aliphatic carbon and nitrogen-containing species) by APPI FT-ICR
20 MS. More recently, Chiaberge *et al.* [10] demonstrated the ability of APCI and APPI FT-ICR MS to
21 detect less polar and apolar bio-oil components whereas ESI FT-ICR MS is more suited for polar
22 species. We have also demonstrated the capability of combining LDI FT-ICR MS and ESI FT-ICR MS
23 analysis to investigate raw or HDO-treated lignin pyrolysis bio-oils [23].

24 Overall, the literature demonstrates that to attain a complete description of a complex
25 mixture, such as bio-oil, complementary ionization techniques must be used. In this study a
26 comprehensive investigation of one complex mixture, an oak pyrolysis bio-oil, was performed using
27 ESI, LDI and APPI. This is the first time such a detailed petroleomic study has been conducted for bio-
28 oil.

29 **2. MATERIALS AND METHODS**

30 **2.1. Bio-oil production**

31 The bio-oil was produced by pyrolysis in a micro-fluidized bed reactor set at 500 °C
32 (temperature of the sand) for 12 min. Two grams of oak powder were continuously injected in to the
33 bed *via* a micro-feeder developed at CNRS Nancy. More details about the process and the raw

1 material composition are available in previous work [35]. The bio-oil was recovered in methanol (the
2 “bio-oil solution”) and stored at -20°C , prior to analysis.

3 **2.2. Preparation of the samples**

4 LCMS grade methanol (VWR–Prolabo), water (Fisher Chemical), and sodium acetate (Fisher
5 Scientific) were used as supplied. For the ESI FT-ICR MS analyses, the bio-oil was diluted to a final
6 concentration of 2% in methanol. Sodium acetate ($0.1\text{ mg}\cdot\text{mL}^{-1}$) was added to favor cationization
7 [33]. For the APPI experiments, the sample is diluted in methanol (4% v/v) without addition of
8 dopant. For LDI experiments, $1\ \mu\text{L}$ of bio-oil/water (70% v/v) solution was deposited on a stainless
9 steel target and dried at room temperature.

10 **2.3. Fourier Transform Ion Cyclotron Resonance Mass Spectrometers**

11 The instrument used for the analyses was a 12 T Solarix FT-ICR equipped with ESI, APPI and
12 LDI sources (Bruker Daltonics). The different ionization methods and operating parameters were
13 optimized via the FTMSControl V2.1.0, build 98 (Bruker Daltonics). Alternatively, some LDI FT-ICR MS
14 measurements were performed on a 9.4 T IonSpec active shielded mass spectrometer.

15 **2.3.1. ESI FT-ICR MS**

16 ESI FT-ICR MS analyses were performed in both positive and negative ion modes. The
17 capillary voltage was set at $\pm 4000\text{ V}$ and the end plate offset at -500 V . The source gas was tuned
18 with nebulizer gas ($1 - 1.8\text{ bar}$), dry gas ($4 - 6\text{ L}\cdot\text{min}^{-1}$) and heated at 180°C . The sample was infused at
19 a flow rate of $200\ \mu\text{L}\cdot\text{h}^{-1}$ into the ion source. The ions were accumulated for 0.3 s per scan and 200
20 analyses were summed to obtain the final mass spectrum in the 129 to 1000 m/z range. The length of
21 the transient was 3 s and the mass resolution was $\approx 680\ 000$ at $m/z\ 400$.

22 **2.3.2. APPI FT-ICR MS**

23 The analyses were performed in positive ion mode with the APPI source equipped with a
24 krypton lamp at 10.6 eV . The voltages of the capillary and the end plate were set at $\pm 1000\text{ V}$ and $-$
25 500 V , respectively. The nebulizer and dry gas were tuned at 1.8 bar and $6\text{ L}\cdot\text{min}^{-1}$ respectively and
26 the source heated to 180°C . The sample was infused at a flow rate of $1\text{ mL}\cdot\text{h}^{-1}$ and the ions were
27 accumulated for 0.05 s . The mass spectra acquired in the 129 to 1000 m/z range were the sum of 100
28 analyses. The transient length was 1.5 s and the mass resolution was $\approx 340\ 000$ at $m/z\ 400$.

29 **2.3.3. LDI FT-ICR MS**

30 The measurements were performed in negative ion mode. Fifty analyses were accumulated
31 to obtain the final mass spectrum in the 147 to 1000 m/z range. Measurements were conducted at

1 the 355 nm wavelength with a diameter of the laser spot of 300 μm . Six hundred laser shots per
2 analysis were accumulated at a 1000 Hz laser frequency. A 1.7s transient length was acquired, which
3 resulted in mass resolution of $\approx 390\,000$ at m/z 400. The power of the laser was optimized to avoid
4 fragmentation and recombination phenomenon [36].

5 Other experiments were performed using a 9.4 T LDI FT-ICR mass spectrometer (IonSpec,
6 Lake Forest, CA). LDI was performed by a Nd:YAG ORION air-cooled laser system (New Wave
7 Research Inc, Fremont, CA) working at 355 nm.

8 The laser power was kept down to 0.7 J cm^{-2} to avoid fragmentation processes and to obtain
9 intense ion signals. A decrease of the laser power did not modify the nature of the detected species
10 but induced a significant decrease in their abundance. The resulting ions from (8 laser shots) were
11 stored in a RF-only hexapole before their transfer to the FT-ICR cell. The ion guide was tuned to
12 optimize the efficient transfer of ions in the m/z 150–500 range into the FT-ICR MS cell. A 1.049 s
13 transient length was acquired with 4096 K data points. Typically, the average mass measurement
14 accuracy was better than 500 ppb, and the mass resolution was between 500 000 and 2 000 000. To
15 increase the signal to noise ratio, each mass spectrum reported in following sections was the sum of
16 45 individual mass spectra.

17 **2.4. Data post-acquisition treatment**

18 The ESI/LDI and APPI FT-ICR MS mass spectra (**S.I. 1** and **S.I. 2**) were analyzed using Data
19 Analysis V4.4, build 102.47.2299 (Bruker Daltonics) and calibrated with well-known oxygenated
20 compounds and a peak list, for each mass spectrum, was generated for all ions with a S/N ratio
21 greater than 4. PetroOrg software (Florida State University) was used for the peak assignment. The
22 attribution parameters were set as following: $\text{C}_{1-100}\text{H}_{2-200}\text{O}_{1-20}\text{N}_{0-20}\text{S}_{0-1}$ (for negative ion mode). Sodium
23 adducts are considered for (+) ESI analyses. The tolerated mass error was ± 1 ppm. The identified
24 peaks and the efficiency of the calibration was checked by the graph representing the mass error
25 against m/z (**S.I. 3**) and the value of the RMS.

26 For 9.4 T LDI FT-ICR MS measurements prior to acquisition, the mass spectrometer was
27 externally calibrated by considering well-known ions such as hydride gold cluster ions. Following
28 acquisition, internal calibration was performed with specific and well characterized $\text{C}_x\text{H}_y\text{O}_{3,4,5}^{+/-}$ ion
29 series. A peak list of signals with a S/N > 4.5 was generated and the Composer software (Sierra
30 Analytics, Modesto, CA) was used for ion assignment with the following search criteria: $\text{C}_{1-100}\text{H}_{1-100}\text{N}_{0-}$
31 $5\text{O}_{0-30}\text{Na}_{0-1}^+$ (positive ion) or $\text{C}_{1-100}\text{H}_{1-100}\text{N}_{0-2}\text{O}_{1-30}\text{S}_{0-1}^-$ (negative ion) general formula, 3 ppm tolerance
32 error, and a double bound equivalent (DBE) ranging from 0 to 40. The recalibration of the mass
33 spectrum was then conducted with signals assigned with an error lower than 1 ppm by considering

1 the following equation with m/z the mass-to-charge ratio, m (uma) the mass and z the charge of the
2 ion, f the measured frequency (Hz) and, A and B the constraints:

$$3 \quad \frac{m}{z} = \frac{A}{f} + \frac{B}{f^2}$$

4 For the non-assigned signals or the assigned signals with an error greater than 1 ppm a
5 manual assignment was conducted by using Omega 8 Elemental Composition software (Varian-
6 IonSpec Inc.) with the previously reported search criteria.

7 Post-treatment was applied to process data to achieve some graphical representations that
8 were necessary in order to compare the results obtained in the different analytical conditions. More
9 specifically, van Krevelen diagrams were used to illustrate the different components of the bio-oil.
10 Each compound was represented by a dot where the x and y coordinate represent its O/C and H/C
11 ratio, respectively. This representation ensures to distinguish species which are relative to lipids (low
12 O/C ratio and H/C ratio close to 2), sugarc derivatives (high O/C and H/C ratios) and pyrolytic
13 products of the lignin (H/C value close to 1 and O/C ratio in the 0.2 to 0.6 range) (S.I. 4)

14 3. RESULTS AND DISCUSSION

15 3.1. ESI FT-ICR MS

16 Whatever the ion detection mode, 95% of the signal is attributed to $C_xH_yO_z$ compounds
17 (Table 1), the composition of which is consistent with the elemental analyses of oak bio-oil [35]. In
18 (+) ESI, the remaining signal is attributed to $C_xH_yNO_z$ compounds whereas in (-) ESI, both $C_xH_yNO_z$ and
19 $C_xH_ySO_z$ species are identified and correspond to 2% and 3% of the total ion signal, respectively. In (+)
20 ESI, NO_z ions are detected as $[M+H]^+$, which corresponds to protonation of the basic sites of the
21 molecule such as amine group or pyridine ring [28]. This is in agreement with the dramatically
22 increase of the signals attributed to nitrogen-containing species when formic acid is added to the
23 sample [33]. NO_z anions are thought to be related to neutral or acidic compounds, which may include
24 for example an indole moiety. It is proposed that the SO_z species are associated with aromatic
25 sulfonated compounds, which easily deprotonate. Alternatively, they may also correspond to HSO_4^-
26 attachment to $C_xH_yO_z$ bio-oil components during the ESI process [37]. The $[M-H]^-$ anion and the
27 $[M+Na]^+$ cation distribution of the $C_xH_yO_z$ bio-oil components present similarities in terms of DBE and
28 the number of oxygen atoms. Nevertheless, differences are highlighted when the relative intensity of
29 these compounds is considered (Figure 1). In (-) ESI, the $[M-H]^-$ ions illustrate a wide variation in the
30 number of oxygen atoms (O2 to O16). The most important signal is observed for O4 to O6
31 compounds. Sodiated cations $[M+Na]^+$ are detected for O1 to O14 bio-oil components, the most
32 abundant signal is obtained for O5 and O6 species and, a bimodal distribution is observed. The
33 second massif is centered on O11 compounds. This behavior has been observed in a previously

1 published work dealing with the study of Miscanthus bio-oil by ESI FT-ICR MS under similar
2 experimental conditions [33]. Furthermore, the van Krevelen diagrams of $C_xH_yO_z$ compounds
3 detected in (-) ESI and (+) ESI are reported in **Figure 2**. Lipids are predominantly observed in (-) ESI
4 but are also observed in (+) ESI. In both ion detection modes, the pyrolytic lignin derivatives
5 constitute the majority of the signal. Nevertheless, (-) ESI analysis reveals a more extended
6 distribution of compounds in terms of unsaturation number and oxygen amounts. The sugarc
7 compounds are more numerous and abundant in (+) ESI. The ability of highly oxygenated compounds
8 to easily poly-coordinated the sodium cation explains this behavior.

9 It has to be noted that these results display significant similarities with the works of
10 Miettinen *et al.* [30] and Jarvis *et al.* [31] who investigated by (-) ESI FT-ICR MS after fractionation
11 the oily and aqueous phases from different pyrolysis bio-oils. Lipids and pyrolytic lignin derivatives
12 were common to both fractions whereas “sugarc species”, which correspond to the most
13 oxygenated compounds, were only highlighted in the aqueous phase. These latter compounds are
14 relative to the second distribution (centered on O11) observed in this study for $[M+Na]^+$ ions. The
15 first massif of the O-containing bio-oil components, common to both ion detection modes, is
16 indicative of the pyrolytic lignin derivatives. In spite of a lower sensitivity of (+) ESI for pyrolytic lignin
17 derivatives and lipids, it is the only experimental condition able to give semi-quantitative information
18 regarding the sugarc and lignin pyrolysis compounds. As a conclusion, both detection modes are
19 useful for the thorough characterization of bio-oil.

20 The comparison of the obtained results with previously published works [15,38,39] can be
21 made to tentatively assign some signals, obtained by (+) or (-) ESI FT-ICR MS (see **S.I. 2a and 2b**), to
22 well-known pyrolysis compounds derived from the wood constituents. Thus, the ions observed at
23 m/z 185.04213, 187.05764 and 347.09467 may be attributed to $[M + Na]^+$ adducts of levoglucosan,
24 glucose and cellobiosan, which are cellulose and hemi-cellulose pyrolysis products. The specific
25 compounds, which derivate from the lignin pyrolysis may also be observed in the form of $[M + Na]^+$
26 and/or $[M - H]^-$. Cinnamic acid and coniferyl aldehyde, two of the lignin paracoumaryl unit derivate
27 are detected as $[M - H]^-$ ion at m/z 147.04512 and 177.05571, respectively. Pyrolysis compounds of
28 guaiacyl (vanillin, eugenol, acetoguaiacon), and syringyl (syringol, methylsyringol, syringaldehyde)
29 units were also evidenced (see S.I.3)

30 **3.2. APPI FT-ICR MS**

31 The predominant part of the total ion current (TIC) observed in (+) APPI, is the results of O-
32 containing compounds. The NO_2 species only represents 10% of the signal. The O_z -species
33 distribution ranges from O1 to O13 with maxima around O6-O7 (**Figure 1**). The corresponding van

1 Krevelen diagram (**Figure 2**) indicates that both lipids and pyrolytic lignin derivatives are observed in
2 APPI. In spite of limited reported data on APPI analyses of woody bio-oils, the comparison with
3 Osborne *et al.* [40] investigation of dissolved organic nitrogen-containing compounds by APPI FT-ICR
4 MS demonstrates that neither proteins nor tannins are detected by (+) APPI FT-ICR MS of pyrolysis
5 bio-oils. As we observed, only lignin derivate compounds and lipids but not cellulose-linked species
6 are detected. Thus, APPI should be considered as inefficient for the ionization of sugarc derivatives.

7 Further examination of (+) APPI mass spectrum, reveals that 75 % of the TIC for O-containing
8 bio-oil components is associated with protonated species and the other species are molecular $M^{•+}$
9 ions. Different ionization pathways may explain the formation of the observed cations, considering
10 that no dopant was added in our (+) APPI experiments. Due to the ionization energy of methanol
11 (10.84 eV), the solvent cannot be directly photoionized by Kr photons (10.6 eV), but the dimer of
12 methanol, corresponding to 2% of the methanol in solution, has a lower ionization energy (9.74 eV)
13 and is efficiently ionized [41]. The radical cation dimer may yield a protonated methanol ion by
14 elimination of a CH_3O^{\bullet} (or $^{\bullet}CH_2OH$) radical. Additionally, the generation of large protonated
15 methanol clusters is facilitated by the large binding energy of neutral CH_3OH to protonate solvent
16 clusters, e.g., CH_3OH binding energy with $[CH_3OH]_nH^+$ is -33 kcal/mol for $n = 1$, -22 kcal/mol for $n =$
17 2 , and -16 kcal/mol for $n = 3$ [42]. The interaction of these protonated methanol clusters with O-
18 containing bio-oil components induces the transfer of the proton, and eventually the fission of the
19 methanol cluster, to the most acidic bio-oil compounds. Wood pyrolysis bio-oils typically have a low
20 pH values and significant amounts of acidic compounds [20]. More specifically, this happens for O/C
21 > 0.4 compounds, which have odd m/z values (**S.I 5**). The formation of even m/z ions may be the
22 result of the direct photoionization, according low ionization energy of highly unsaturated and
23 conjugated species or charge transfer from the $[CH_3OH]_2^{•+}$ ion. Alternatively, part of the large
24 number of the bio-oil components may act as a self-dopant. It has to be noted that the addition of a
25 typical APPI dopant (toluene) had no significant effect on the obtained mass spectrum.

26 **3.3. LDI FT-ICR MS**

27 The experiments were conducted in both positive and negative mode. In this latter case,
28 both 9.4 T and 12 T instruments were used. The majority of detected ions are O-containing
29 compounds, independent of the instrument or the ion detection mode used. This observation is
30 more pronounced in negative LDI FT-ICR MS for which the obtained distribution with the 12 T
31 instrument is $C_xH_yO_z$ (92 %), $C_xH_yNO_z$ (3%) and $C_xH_ySO_z$ (5%) and $C_xH_yO_z$ (97 %), $C_xH_yNO_z$ (3%) and
32 $C_xH_ySO_z$ (0.3%) for the 9.4 T FT-ICR mass spectrometer (**Table 1**). The distribution of O-containing
33 species presents a maximum at O6 components in negative ion detection mode. A broad distribution
34 of the number of oxygen atoms is observed for the 12 T instrument (from O3 to O17); whereas the

1 mass spectrum obtained with the 9.4 T mass spectrometer limits the distribution to 10 oxygen
2 atoms. In (+) LDI, the signal is relative to $C_xH_yO_z$ (83% of the TIC) and $C_xH_yNO_z$ (17% of the TIC)
3 compounds. The O-containing compounds ranges from O2 to O14 with maxima observed for O4 – O5
4 species (Figure 1). The species containing 8 to 14 oxygen atoms are detected as sodium adducts.
5 These sodium ions originate from the solvents used in the analysis. In gas phase, Na^+ easily
6 coordinates with low unsaturated compounds which contain a significant amount of oxygen atoms.

7 According to the O/C and H/C ratios, both pyrolytic lignin derivatives and sugarc compounds
8 (but not lipids) are detected on the 12 T (-) LDI mass spectrum (Figure 2). The 9.4 T (-) LDI, leads to
9 the specific observation of the pyrolytic lignin compounds (Figure 2). Lignin linked compounds are
10 observed in the LDI experiments due to their significant absorption properties at the laser
11 wavelength used. This is confirmed by previous work carried out by Olcese *et al.* [23] who
12 investigated bio-oils produced by pyrolysis of lignin for which O2 to O8 compounds with DBE values
13 ranging from 7 to 25 were observed. Smith *et al.* [29] also observed that O4, O5 and O6 were the
14 main O-containing bio-oil component observed by LDI–Orbitrap MS. Differences in (-) LDI results
15 obtained with the 12 T and 9.4 T instruments can be explained with the different 355 nm laser
16 profiles of both setups. The energy surface distribution of the smartbeam™ laser which is coupled
17 with the 12 T FT-ICR MS instrument is less homogeneous than the Orion. Indeed, the “average
18 homogeneity” of the smartbeam™ is obtained by the repetition on the same area of a large number
19 of different laser shots [43]. For the Orion laser, each laser shot is more homogeneous. As a
20 consequence, the smartbeam laser leads to the formation of hot (and cold) spots, for which the laser
21 energy may be higher (and lower) than the laser energy deposited at the surface of the sample by
22 the Orion laser. Typically, the compounds which have low absorption properties (in this case sugarc
23 compounds) need high laser energy to be desorbed and ionized. Such conditions occur in the hot
24 spots of the smartbeam™ laser but not with the homogeneous Orion laser.

25 In LDI, compounds are detected as radical or protonated/deprotonated ions. The radicals are
26 highly unsaturated compounds ($H/C < 1$) with $O/C < 0.4$, as shown in S.I. 5. Among the O-containing
27 species, only 4% of the signal is attributed to $M^{\bullet-}$ ions using the 12 T mass spectrometer (S.I. 4).
28 Whereas, when using the 9.4 T equipped with the Orion laser, they represent 22% ($M^{\bullet+}$) and 15%
29 ($M^{\bullet-}$). It is proposed that these differences are linked to the laser-sample interaction which is
30 strongly dependent on the laser beam as previously mentioned.

31 3.4. Complementarity of the different ionization sources

32 Irrespective of the ionization method used and the ion detection mode, the obtained
33 compound class distribution is mainly associated with O-contained compounds, which is consistent
34 with CHNOS elemental analysis, at least 90% of the TIC is related to $C_xH_yO_z$ compounds (Table 1).

1 Nitrogen species are always detected while SO₂ compounds are only detected in negative ion
2 detection mode. **Figures 2 and 3** well illustrate the complexity of the bio-oil samples and the
3 complementarity of ESI, APPI and LDI sources for their ionization and analysis.

4 **3.4.1. Positive ion mode analyses**

5 The distributions of the O-species achieved in (+) ESI and (+) APPI appear very similar based
6 on the importance of O₂ bio-oil components (**Table 1**), which extend to a similar range from O1 to
7 O14 and from O1 to O13, respectively. However, further insight can be gained by assessing the
8 intensity of the DBE distribution for each heteroatom class (**Figure 1**). In ESI, the most intense
9 compounds detected contain 10 and 11 oxygen atoms and have DBE < 5. The other prominent
10 species are composed of 5 to 7 oxygen atoms and their DBE values range from 0 to 5. The most
11 oxygenated species have the properties of pyrolytic sugarc derivatives whereas the less oxygenated
12 ones are pyrolytic lignin derivatives and lipids, these components were also evidenced on a
13 Miscanthus bio-oil in (+) ESI [33]. On the other hand, in case of APPI, compounds having 10 or more
14 oxygen atoms are not significant which means that sugarc compounds are not ionized in APPI.
15 However, species containing 4 to 8 oxygen atoms are intensely detected, which is also seen using ESI.
16 But their unsaturation degree is much more important, with DBE ranging between 5 and 20. These
17 molecular properties can be attributed to pyrolytic lignin derivatives and lipids. Moreover,
18 compounds identified in ESI contain up to 30 carbon atoms on a mass range of *m/z* 150 to 600
19 whereas in APPI, they have up to 40 carbon atoms and a mass range from *m/z* 200 to 800.

20 Thus, APPI is useful to observe the highest mass-to-charge-ratio compounds with high DBE
21 values and low polarity (not observed on (+) ESI mass spectrum). Nevertheless, these hetero-
22 polyaromatic compounds are not totally apolar due to their capability to be ionized in APPI by
23 protonation rather than charge transfer. ESI is a suitable method to observe polar to middle polar
24 compounds which are characterized by a low unsaturation degree and a significant amount of
25 heteroatoms such as oxygen in the case of bio-oils [10,13,16]. The (+) LDI analysis yields results very
26 similar to those obtained by (+) ESI and (+) APPI. It leads to an intermediate behavior and allows both
27 middle polar to low polar bio-oil components to be observed at the exception of the high mass
28 species. The combination of the different used ionization methods is consequently well suited to
29 exhaustively describe pyrolytic bio-oil.

30 The examination of the obtained signals in respect to the DBE value and the number of
31 oxygen atoms for the three different ionization techniques **Figure 1** highlights that positive ESI is
32 more sensitive to ionization competition. More specifically, highly saturated compounds with high
33 levels of oxygen are well suited to form stable sodium adducts which lead to the increase of the
34 associated signal. The same kind of discrimination is observed with components presenting a high

1 proton affinity when bio-oil is directly infused in the ESI source. In contrast, positive APPI and in a
2 lesser extent positive LDI lead to a less compound-dependent ionization and ensure a more precise
3 description of the bio-oil component distribution to be obtained but only on pyrolytic lignin species.

4 **3.4.2. Negative ion mode analyses**

5 The $C_xH_yO_z$ compound distributions obtained in (-) ESI and (-) LDI are very similar in respect
6 with the oxygen atom amounts (**Figure 1**). In both ionization modes, a broad O-class of compounds
7 are detected, with O2-O16 components in (-) ESI and O3-O17, in (-) LDI using the 12 T FT-ICR MS.
8 The O-species range obtained with the 9.4 T FT-ICR MS is narrower (O3 to O10 oxygen atoms).
9 However, when using either instrument, the O4 to O6 species are the most predominant. These
10 observed trends are very similar to those obtained in positive detection mode with ESI, LDI and APPI.
11 As shown in **Figure 1**, degree of unsaturation is more important for compounds detected in LDI than
12 those in ESI. These results are consistent with published literature. For example, the LDI and ESI
13 analyses of extracts from fast pyrolysis char obtained by Cole *et al.* [17] present similar distribution of
14 compounds in respect to their heteroatom classes with a DBE distribution centered at higher values
15 in LDI. Consequently, this behavior has to be considered as a generalization for woody bio-oils of
16 what we previously reported for lignin pyrolysis products [23]. Thus, negative LDI exhibits the
17 capability to efficiently ionize low to medium polar compounds presenting different amounts of
18 oxygen atoms and a high number of unsaturation, which is due to the absorption properties at the
19 wavelength of the ionization laser, whereas negative ESI is more suited to more polar species such as
20 lipids.

21 The comparison of positive and negative mode van Krevelen diagrams for lignin derivate
22 compounds is also of significant interest. The O/C ratio is very similar and generally ranges from 0.1
23 to 0.7. In contrast, the H/C ratio varies significantly. For LDI and APPI, this ratio for the observed
24 compounds is centered on 1, in contrast it is significantly higher in positive ESI and lower in negative
25 ESI. ESI ensures the efficient ionization of polar compounds, positive ESI is sensitive to basic
26 compounds whereas negative ESI is well suited to neutral or acidic species. APPI and LDI are less
27 sensitive to these differences in chemical properties and as a consequence, the acidic and neutral
28 fraction of bio-oil is predominantly highly unsaturated species, which easily deprotonated to produce
29 anions stabilized by significant mesomeric effects.

30 The complementarity of the ionization sources is also assessed by the Venn diagrams giving
31 the repartition of the different 4500 compound formulae depending on the ionization source and the
32 ion polarity (**Figure 3**). In positive ion mode (**Figure 3a**), APPI enabled to identify 1297 exclusive
33 formulae whereas ESI and LDI allowed to attribute 449 and 92 own formulae, respectively. As a
34 result, only 65 compounds were common to the 3 ionization sources. Besides, the same

1 representation was done in negative ion mode (**Figure 3b**), with ESI and LDI. It appeared that 617
2 formulae were specific to ESI, and 625 to LDI in the best conditions. Finally, as (-) ESI has been the
3 only ionization method in most bio-oil analyses [22], it is clearly demonstrated here that this strategy
4 nearly highlights 1250/4500 elemental formulae corresponding to less than 28% of the total bio-oil
5 components.

6 **4. CONCLUDING REMARKS**

7 Comprehensive petroleomic analysis of bio-oil by ESI, APPI and LDI FT-ICR MS, showed that
8 the heteroatom distributions as obtained by these three different methods were very similar. In fact,
9 for any given ion detection mode, the $C_xH_yO_z$ species are the most abundant compound family and
10 their distributions extend across comparable ranges of oxygen atom numbers. However, when
11 focused on the DBE distributions obtained for each of the ionization modes, some differences
12 became apparent. In ESI, the compounds were more highly saturated, with $2 < \text{DBE} < 10$, whereas in
13 APPI, they were more unsaturated with $5 < \text{DBE} < 20$. In LDI, the range of unsaturation was between
14 those obtained by ESI and APPI but it was also affected by the FT-ICR MS laser configuration. With a
15 non-homogeneous laser beam, components identified were less unsaturated

16 This approach successfully demonstrated that the characterization of complex mixtures by
17 non-targeted analysis required the use of different but complementary ionization sources in order to
18 have the most exhaustive as possible description. Indeed, at the maximum, the common used
19 negative ESI only allowed the MS detection of less than 28% of the combined features obtained by
20 ESI, APPI and LDI FT-ICR MS.

21 **ACKNOWLEDGMENTS**

22 The authors, more especially Jasmine Hertzog, would like to thank the European COST Action
23 1306 "Lignoal" for its financial support, as it enabled a new collaboration between the LCP-A2MC,
24 Université de Lorraine and the UK Biochar Research Center, Edinburgh University. The analyses with
25 the 9.4 T FT-ICR MS were performed at the LCP-A2MC whereas the measurements carried out with
26 the 12 T FT-ICR MS were done at the Scottish Instrumentation and Resource Centre for Advanced
27 Mass Spectrometry (SIRCAMS) at the University of Edinburgh. The TGIR program FR 3624,
28 infrastructure program of CNRS, is acknowledged for further financial support. Authors also thank Dr
29 Faye Cruickshank for her valuable editing of the manuscript.

1 REFERENCES

- 2 [1] P.M. Medeiros, B.R.T. Simoneit, Analysis of sugars in environmental samples by gas
3 chromatography–mass spectrometry, *J. Chromatogr. A.* 1141 (2007) 271–278.
4 doi:10.1016/j.chroma.2006.12.017.
- 5 [2] Y.S. Choi, P.A. Johnston, R.C. Brown, B.H. Shanks, K.-H. Lee, Detailed characterization of red
6 oak-derived pyrolysis oil: Integrated use of GC, HPLC, IC, GPC and Karl-Fischer, *J. Anal. Appl.*
7 *Pyrolysis.* 110 (2014) 147–154. doi:10.1016/j.jaap.2014.08.016.
- 8 [3] P. Jonsson, A.I. Johansson, J. Gullberg, J. Trygg, J. A, B. Grung, S. Marklund, M. Sjöström, H.
9 Antti, T. Moritz, High-Throughput Data Analysis for Detecting and Identifying Differences
10 between Samples in GC/MS-Based Metabolomic Analyses, *Anal. Chem.* 77 (2005) 5635–5642.
11 doi:10.1021/ac050601e.
- 12 [4] J. Peng, J.E. Elias, C.C. Thoreen, L.J. Licklider, S.P. Gygi, Evaluation of Multidimensional
13 Chromatography Coupled with Tandem Mass Spectrometry (LC/LC–MS/MS) for Large-Scale
14 Protein Analysis: The Yeast Proteome, *J. Proteome Res.* 2 (2003) 43–50.
15 doi:10.1021/pr025556v.
- 16 [5] K. Fraser, S.J. Harrison, G.A. Lane, D.E. Otter, Y. Hemar, S.-Y. Quek, S. Rasmussen, Non-targeted
17 analysis of tea by hydrophilic interaction liquid chromatography and high resolution mass
18 spectrometry, *Food Chem.* 134 (2012) 1616–1623. doi:10.1016/j.foodchem.2012.03.045.
- 19 [6] K. Hanhineva, I. Rogachev, H. Kokko, S. Mintz-Oron, I. Venger, S. Kärenlampi, A. Aharoni, Non-
20 targeted analysis of spatial metabolite composition in strawberry (*Fragaria × ananassa*) flowers,
21 *Phytochemistry.* 69 (2008) 2463–2481. doi:10.1016/j.phytochem.2008.07.009.
- 22 [7] J.S. Sampson, A.M. Hawkrigde, D.C. Muddiman, Generation and Detection of Multiply-Charged
23 Peptides and Proteins by Matrix-Assisted Laser Desorption Electrospray Ionization (MALDESI)
24 Fourier Transform Ion Cyclotron Resonance Mass Spectrometry, *J. Am. Soc. Mass Spectrom.* 17
25 (2006) 1712–1716. doi:10.1016/j.jasms.2006.08.003.
- 26 [8] C.A. Hughey, R.P. Rodgers, A.G. Marshall, Resolution of 11 000 Compositionally Distinct
27 Components in a Single Electrospray Ionization Fourier Transform Ion Cyclotron Resonance
28 Mass Spectrum of Crude Oil, *Anal. Chem.* 74 (2002) 4145–4149. doi:10.1021/ac020146b.
- 29 [9] D. Cao, H. Huang, M. Hu, L. Cui, F. Geng, Z. Rao, H. Niu, Y. Cai, Y. Kang, Comprehensive
30 characterization of natural organic matter by MALDI- and ESI-Fourier transform ion cyclotron
31 resonance mass spectrometry, *Anal. Chim. Acta.* 866 (2015) 48–58.
32 doi:10.1016/j.aca.2015.01.051.
- 33 [10] S. Chiaberge, I. Leonardis, T. Fiorani, P. Cesti, S. Reale, F. De Angelis, Bio-Oil from Waste: A
34 Comprehensive Analytical Study by Soft-Ionization FTICR Mass Spectrometry, *Energy Fuels.* 28
35 (2014) 2019–2026. doi:10.1021/ef402452f.
- 36 [11] A.G. Marshall, R.P. Rodgers, *Petroleomics: The Next Grand Challenge for Chemical Analysis,*
37 *Acc. Chem. Res.* 37 (2004) 53–59. doi:10.1021/ar020177t.
- 38 [12] J.A. Hawkes, T. Dittmar, C. Patriarca, L. Tranvik, J. Bergquist, Evaluation of the Orbitrap Mass
39 Spectrometer for the Molecular Fingerprinting Analysis of Natural Dissolved Organic Matter,
40 *Anal. Chem.* 88 (2016) 7698–7704. doi:10.1021/acs.analchem.6b01624.
- 41 [13] M. Staš, J. Chudoba, D. Kubička, M. Pospíšil, Chemical Characterization of Pyrolysis Bio-oil:
42 Application of Orbitrap Mass Spectrometry, *Energy Fuels.* 29 (2015) 3233–3240.
43 doi:10.1021/acs.energyfuels.5b00407.
- 44 [14] R. Breitling, A.R. Pitt, M.P. Barrett, Precision mapping of the metabolome, *Trends Biotechnol.*
45 24 (2006) 543–548. doi:10.1016/j.tibtech.2006.10.006.
- 46 [15] E. Alsbou, B. Helleur, Direct Infusion Mass Spectrometric Analysis of Bio-oil Using ESI-Ion-Trap
47 MS, *Energy Fuels.* 28 (2014) 578–590. doi:10.1021/ef4018288.
- 48 [16] S. Lababidi, W. Schrader, Online normal-phase high-performance liquid
49 chromatography/Fourier transform ion cyclotron resonance mass spectrometry: Effects of
50 different ionization methods on the characterization of highly complex crude oil mixtures,
51 *Rapid Commun. Mass Spectrom.* 28 (2014) 1345–1352. doi:10.1002/rcm.6907.

- 1 [17] D.P. Cole, E.A. Smith, Y.J. Lee, High-Resolution Mass Spectrometric Characterization of
2 Molecules on Biochar from Pyrolysis and Gasification of Switchgrass, *Energy Fuels*. 26 (2012)
3 3803–3809. doi:10.1021/ef300356u.
- 4 [18] J. Lédé, F. Broust, F.-T. Ndiaye, M. Ferrer, Properties of bio-oils produced by biomass fast
5 pyrolysis in a cyclone reactor, *Fuel*. 86 (2007) 1800–1810. doi:10.1016/j.fuel.2006.12.024.
- 6 [19] A.V. Bridgwater, Review of fast pyrolysis of biomass and product upgrading, *Biomass Bioenergy*.
7 38 (2012) 68–94. doi:10.1016/j.biombioe.2011.01.048.
- 8 [20] D. Vamvuka, Bio-oil, solid and gaseous biofuels from biomass pyrolysis processes—An
9 overview, *Int. J. Energy Res.* 35 (2011) 835–862. doi:10.1002/er.1804.
- 10 [21] M. Stas, D. Kubicka, J. Chudoba, M. Pospisil, Overview of Analytical Methods Used for Chemical
11 Characterization of Pyrolysis Bio-oil, *Energy Fuels*. 28 (2014) 385–402. doi:10.1021/ef402047y.
- 12 [22] C.M. Michailof, K.G. Kalogiannis, T. Sfetsas, D.T. Patiaka, A.A. Lappas, Advanced analytical
13 techniques for bio-oil characterization, *Wiley Interdiscip. Rev. Energy Environ.* (2016) n/a-n/a.
14 doi:10.1002/wene.208.
- 15 [23] R. Olcese, V. Carré, F. Aubriet, A. Dufour, Selectivity of Bio-oils Catalytic Hydrotreatment
16 Assessed by Petroleomic and GC*GC/MS-FID Analysis, *Energy Fuels*. 27 (2013) 2135–2145.
17 doi:10.1021/ef302145g.
- 18 [24] Y. Bi, G. Wang, Q. Shi, C. Xu, J. Gao, Compositional Changes during Hydrodeoxygenation of
19 Biomass Pyrolysis Oil, *Energy Fuels*. 28 (2014) 2571–2580. doi:10.1021/ef4024405.
- 20 [25] N. Sudasinghe, J.R. Cort, R. Hallen, M. Olarte, A. Schmidt, T. Schaub, Hydrothermal liquefaction
21 oil and hydrotreated product from pine feedstock characterized by heteronuclear two-
22 dimensional NMR spectroscopy and FT-ICR mass spectrometry, *Fuel*. 137 (2014) 60–69.
23 doi:10.1016/j.fuel.2014.07.069.
- 24 [26] P.V. Abdelnur, B.G. Vaz, J.D. Rocha, M.B.B. de Almeida, M.A.G. Teixeira, R.C.L. Pereira,
25 Characterization of Bio-oils from Different Pyrolysis Process Steps and Biomass Using High-
26 Resolution Mass Spectrometry, *Energy Fuels*. 27 (2013) 6646–6654. doi:10.1021/ef400788v.
- 27 [27] N.S. Tessarolo, R.C. Silva, G. Vanini, A. Pinho, W. Romão, E.V.R. de Castro, D.A. Azevedo,
28 Assessing the chemical composition of bio-oils using FT-ICR mass spectrometry and
29 comprehensive two-dimensional gas chromatography with time-of-flight mass spectrometry,
30 *Microchem. J.* 117 (2014) 68–76. doi:10.1016/j.microc.2014.06.006.
- 31 [28] D.P. Cole, E.A. Smith, D. Dalluge, D.M. Wilson, E.A. Heaton, R.C. Brown, Y.J. Lee, Molecular
32 characterization of nitrogen-containing species in switchgrass bio-oils at various harvest times,
33 *Fuel*. 111 (2013) 718–726. doi:10.1016/j.fuel.2013.04.064.
- 34 [29] E.A. Smith, Y.J. Lee, Petroleomic Analysis of Bio-oils from the Fast Pyrolysis of Biomass: Laser
35 Desorption Ionization–Linear Ion Trap–Orbitrap Mass Spectrometry Approach, *Energy Fuels*. 24
36 (2010) 5190–5198. doi:10.1021/ef100629a.
- 37 [30] I. Miettinen, M. Mäkinen, T. Vilppo, J. Jänis, Compositional Characterization of Phase-Separated
38 Pine Wood Slow Pyrolysis Oil by Negative-Ion Electrospray Ionization Fourier Transform Ion
39 Cyclotron Resonance Mass Spectrometry, *Energy Fuels*. (2015). doi:10.1021/ef5025966.
- 40 [31] J.M. Jarvis, A.M. McKenna, R.N. Hilten, K.C. Das, R.P. Rodgers, A.G. Marshall, Characterization of
41 Pine Pellet and Peanut Hull Pyrolysis Bio-oils by Negative-Ion Electrospray Ionization Fourier
42 Transform Ion Cyclotron Resonance Mass Spectrometry, *Energy Fuels*. 26 (2012) 3810–3815.
43 doi:10.1021/ef300385f.
- 44 [32] Y. Liu, Q. Shi, Y. Zhang, Y. He, K.H. Chung, S. Zhao, C. Xu, Characterization of Red Pine Pyrolysis
45 Bio-oil by Gas Chromatography–Mass Spectrometry and Negative-Ion Electrospray Ionization
46 Fourier Transform Ion Cyclotron Resonance Mass Spectrometry, *Energy Fuels*. 26 (2012) 4532–
47 4539. doi:10.1021/ef300501t.
- 48 [33] J. Hertzog, V. Carré, Y. Le Brech, A. Dufour, F. Aubriet, Toward Controlled Ionization Conditions
49 for ESI-FT-ICR-MS Analysis of Bio-Oils from Lignocellulosic Material, *Energy Fuels*. 30 (2016)
50 5729–5739. doi:10.1021/acs.energyfuels.6b00655.
- 51 [34] I. Leonardis, S. Chiaberge, T. Fiorani, S. Spera, E. Battistel, A. Bosetti, P. Cesti, S. Reale, F. De
52 Angelis, Characterization of Bio-oil from Hydrothermal Liquefaction of Organic Waste by NMR

1 Spectroscopy and FTICR Mass Spectrometry, *Chemoschem.* 6 (2013) 160–167.
2 doi:10.1002/cssc.201200314.

3 [35] Y. Le Brech, L. Jia, S. Cissé, G. Mauviel, N. Brosse, A. Dufour, Mechanisms of biomass pyrolysis
4 studied by combining a fixed bed reactor with advanced gas analysis, *J. Anal. Appl. Pyrolysis.*
5 117 (2016) 334–346. doi:10.1016/j.jaap.2015.10.013.

6 [36] S. Schramm, V. Carré, J.-L. Scheffler, F. Aubriet, Analysis of Mainstream and Sidestream
7 Cigarette Smoke Particulate Matter by Laser Desorption Mass Spectrometry, *Anal. Chem.* 83
8 (2011) 133–142. doi:10.1021/ac1019842.

9 [37] Y. Jiang, R.B. Cole, Oligosaccharide analysis using anion attachment in negative mode
10 electrospray mass spectrometry, *J. Am. Soc. Mass Spectrom.* 16 (2005) 60–70.
11 doi:10.1016/j.jasms.2004.09.006.

12 [38] A. Le Masle, D. Angot, C. Gouin, A. D’Attoma, J. Ponthus, A. Quignard, S. Heinisch, Development
13 of on-line comprehensive two-dimensional liquid chromatography method for the separation
14 of biomass compounds, *J. Chromatogr. A.* 1340 (2014) 90–98.
15 doi:10.1016/j.chroma.2014.03.020.

16 [39] M. Staš, J. Chudoba, M. Auersvald, D. Kubička, S. Conrad, T. Schulzke, M. Pospíšil, Application of
17 orbitrap mass spectrometry for analysis of model bio-oil compounds and fast pyrolysis bio-oils
18 from different biomass sources, *J. Anal. Appl. Pyrolysis.* (n.d.). doi:10.1016/j.jaap.2017.02.002.

19 [40] D.M. Osborne, D.C. Podgorski, D.A. Bronk, Q. Roberts, R.E. Sipler, D. Austin, J.S. Bays, W.T.
20 Cooper, Molecular-level characterization of reactive and refractory dissolved natural organic
21 nitrogen compounds by atmospheric pressure photoionization coupled to Fourier transform ion
22 cyclotron resonance mass spectrometry, *Rapid Commun. Mass Spectrom.* 27 (2013) 851–858.
23 doi:10.1002/rcm.6521.

24 [41] L.C. Short, S.-S. Cai, J.A. Syage, APPI-MS: Effects of Mobile Phases and VUV Lamps on the
25 Detection of PAH Compounds, *J. Am. Soc. Mass Spectrom.* 18 (2007) 589–599.
26 doi:10.1016/j.jasms.2006.11.004.

27 [42] E. Grimsrud, P. Kebarle, Gas-Phase Ion Equilibria Studies of Solvation of Hydrogen-Ion by
28 Methanol, Dimethyl Ether, and Water - Effect of Hydrogen-Bonding, *J. Am. Chem. Soc.* 95
29 (1973) 7939–7943. doi:10.1021/ja00805a002.

30 [43] A. Holle, A. Haase, M. Kayser, J. Höhdorf, Optimizing UV laser focus profiles for improved
31 MALDI performance, *J. Mass Spectrom.* 41 (2006) 705–716. doi:10.1002/jms.1041.

32

1 **CAPTION**

2 **Table 1:** Relative distribution of compound families identified in bio-oil using positive and negative
3 detection mode in ESI, LDI and APPI FT-ICR MS.

4 **Figure 1:** Relative intensities of the $C_xH_yO_z$ compounds in (+) and (-) ESI, APPI and LDI FT-ICR MS
5 spectra of wood-derived bio-oil according to the DBE and oxygen atom distributions

6 **Figure 2:** Relative intensities of the $C_xH_yO_z$ compounds in wood-derived bio-oil represented on the
7 van Krevelen diagrams according to their H/C and O/C ratios as obtained by (+) and (-) ESI,
8 APPI and LDI FT-ICR MS.

9 **Figure 3:** Venn diagrams of $C_xH_yO_z$ compounds in wood-derived bio-oil obtained in (a) positive ion
10 mode and (b) negative ion mode.

1 **Table 1**

2

3

4

5

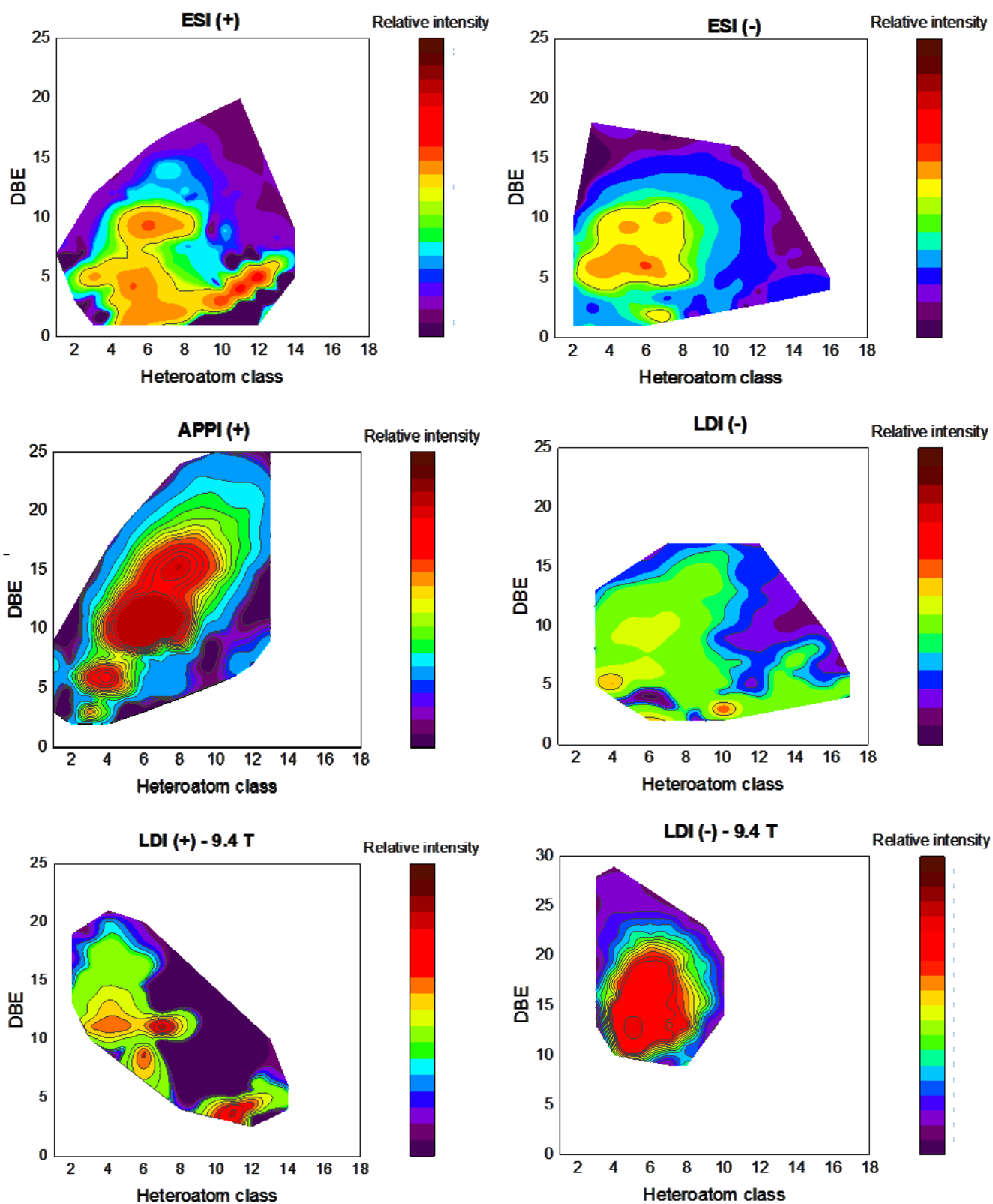
6

7

| | # ¹² C identified compounds | C _x H _y O _z | C _x H _y NO _z | C _x H _y SO _z |
|-----------|--|--|---|---|
| ESI (+) | 1521 | 95% | 5% | – |
| ESI (-) | 1382 | 95% | 2% | 3% |
| APPI (+) | 2778 | 90% | 10% | – |
| LDI (-) | 936 | 92% | 3% | 5% |
| LDI (+) * | 415 | 83% | 17% | – |
| LDI (-) * | 1222 | 97% | 3% | – |

* 9.4T FT-ICR MS

1 **Figure 1**

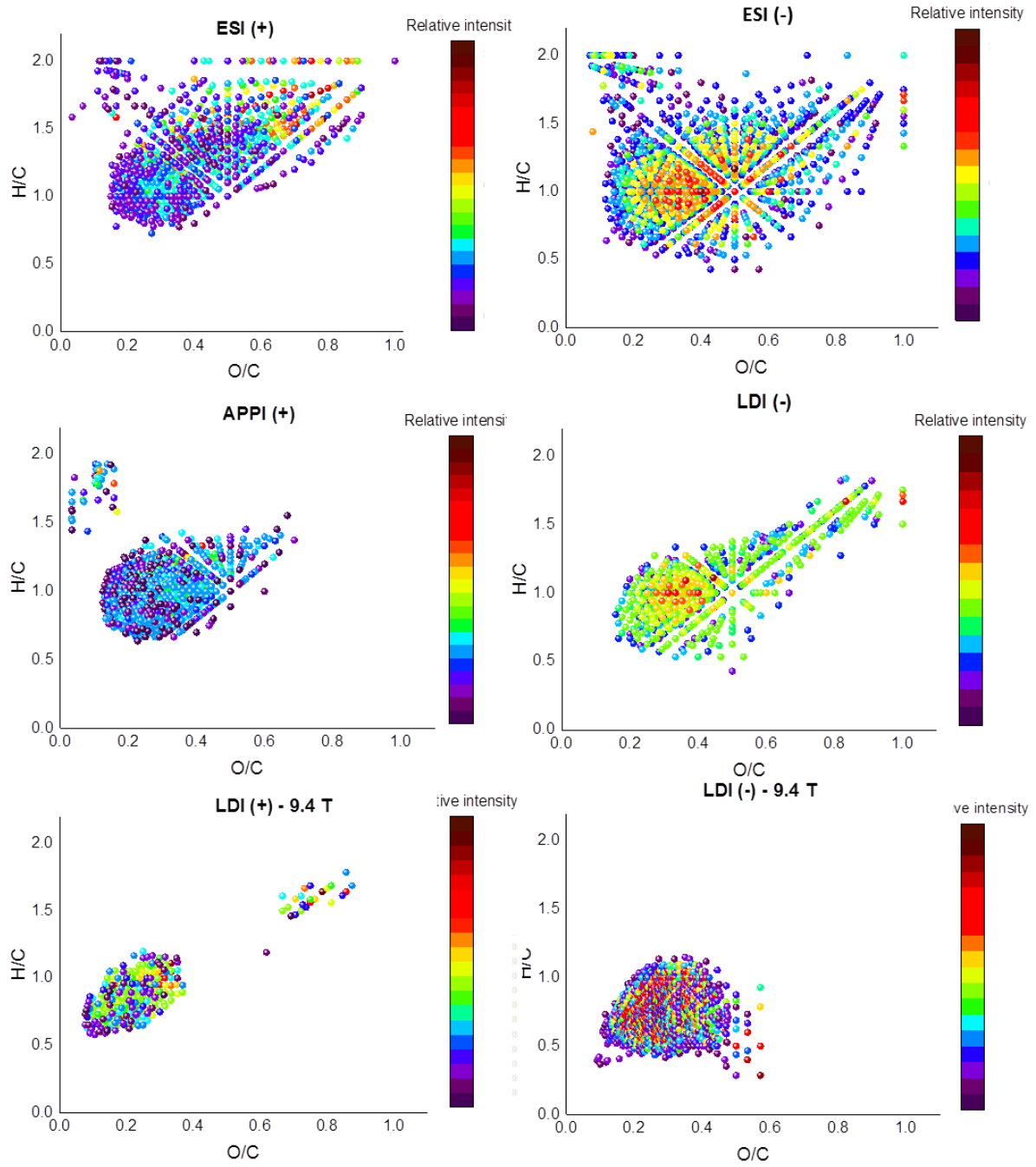


2
3

4 Color for online only

1 **Figure 2**

2



3

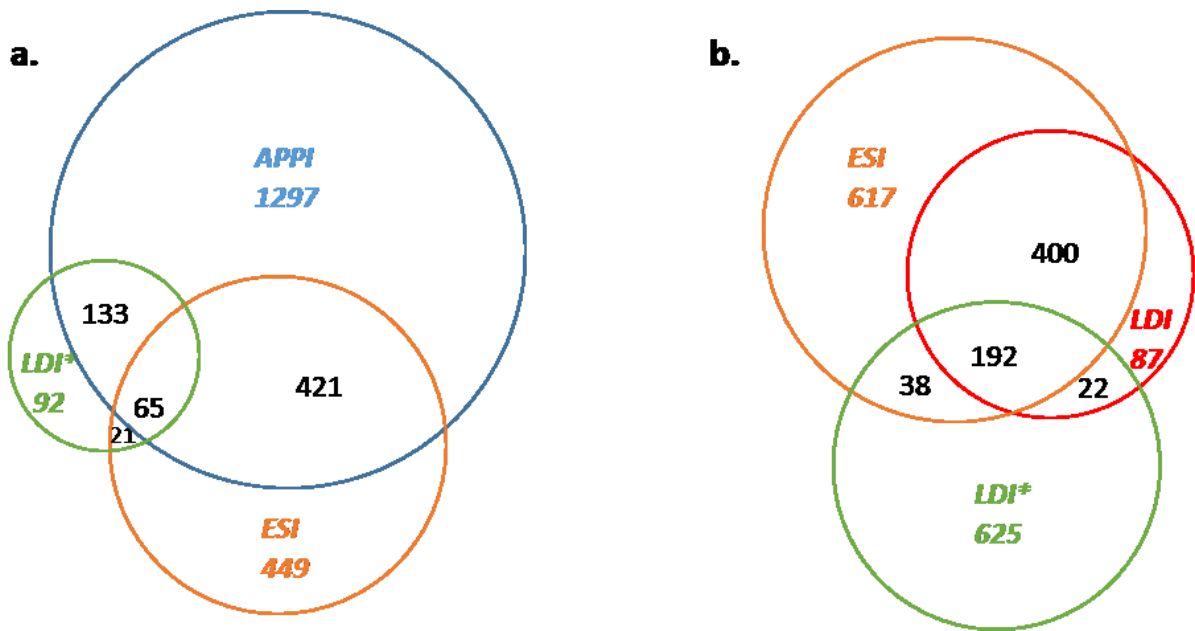
4

5

6 Color for online only

1 **Figure 3**

2



3

4 * 9.4T FT-ICR MS

5

6

7 Color for online only